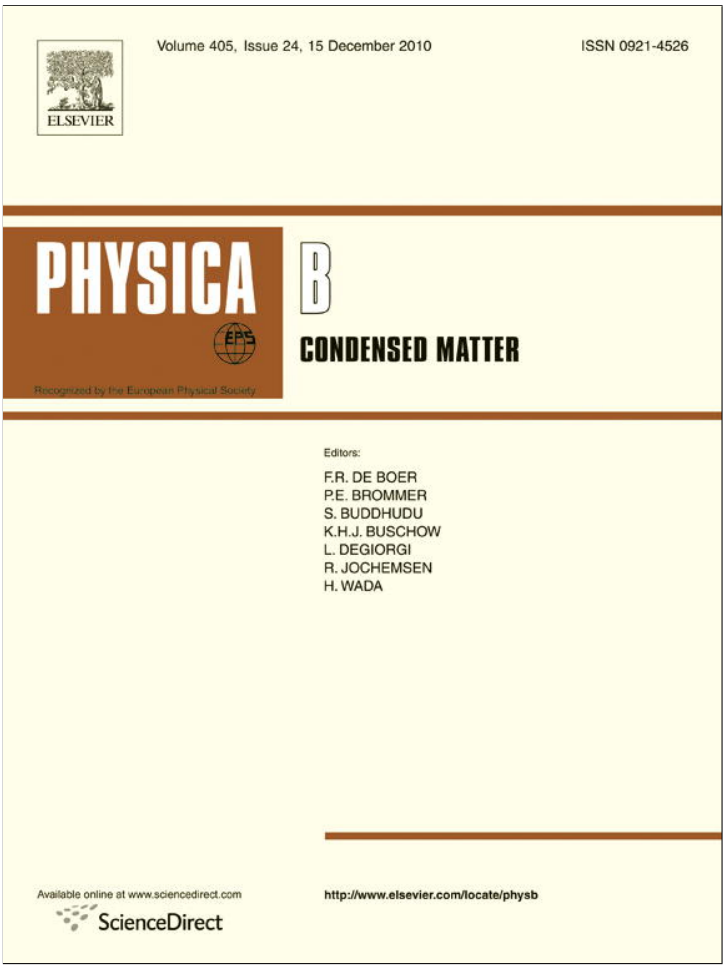

Physica B 405 (2010) 4937–4942

Contents lists available at ScienceDirect

Physica B

journal homepage: www.elsevier.com/locate/physb

Influence of 3d transition metals (Fe, Co) on the structural, electrical and magnetic properties of C_{60} nano-cage

M. Bezi Javan, N. Tajabor, M. Behdani, M. Rezaee Rokn-Abadi *

Physics Department, Ferdowsi University of Mashhad, Mashhad, Iran

ARTICLE INFO

Article history:
Received 29 August 2010
Received in revised form
23 September 2010
Accepted 24 September 2010

Keywords:
Transition metal
Endohedral fullerene
Exohedral fullerene
Heterofullerene

ABSTRACT

Total energy calculations of C_{60} nano-cage doped with transition metals (TM=Fe and Co atoms) endohedrally, exohedrally, and substitutionally were performed using the density functional theory with the generalized gradient approximation along five radial paths inside and outside of the fullerene. The full geometry optimization near the minimum of the binding energy curves shows that the most stable position of the Fe atom in the TM@C_{60} system is below the carbon atom, while that of the Co atom is below the middle of the double bond between the carbon atoms. Also the most stable position of both TM atoms in TM: C_{60} systems is above the double bond. Results reveal that for all examined structures, the Co atom has larger binding energy than that of Fe atom. It is also found that for all complexes additional peaks contributed by TM-3d, 4s and 4p states appear in the highest occupied molecular orbital (HOMO) and the lowest unoccupied molecular orbital (LUMO) gap of the host cluster. The mid-gap states are mainly due to the hybridization between TM-3d, 4s and 4p orbitals and the cage π orbitals. Because of the interaction between the TM atom and the fullerene cage, the charge depletion of TM-4s orbital to TM-3d and 4p orbitals occurs and the magnetic moment of the incorporated TM atom reduces in all cases. Furthermore, the Mulliken charge population analysis shows that overall charge transfer occurs from the TM atom to the cage.

1. Introduction

Fullerene, the hollow carbon cage, discovered in 1958 [1], has greatly influenced contemporary chemistry. The most prominent representative of the fullerene class is C_{60}, which is the most abundant cluster in the solvent-extracted carbon soot and the smallest fullerene that satisfies the isolated pentagon rule (IPR). The IPR is based on the finding that fullerenes with isolated pentagonal rings are kinetically more stable than those with conjugated pentagonal rings due to the high chemical reactivity and strain of the fused pentagonal rings [2]. So far numerous scientific researchers have been carried out relating to the interaction of the fullerene cage with foreign atoms [3–8]. Doping fullerene with foreign atoms can alter the properties of these systems by enhancing their chemical reactivity while maintaining their stable closed three dimensional structures. Exohedral doping on the fullerene has led to the well known superconductivity of fullerides [9]. There are two other ways of doping C_{60}: (1) doping on the inside of the fullerene molecules (endohedral fullerenes) and (2) replacing one or more carbon atoms of the fullerene molecules with heteroatoms (heterofullerene) [10]. In the past several years, some work has been done on doping C_{60} using alkali, transition and rare earth metals [11–15]. Because of their valance level structures such as ns, $(n-1)d$ and $(n-2)f$, they may exhibit different spin configurations. In this work we studied the electronic and magnetic properties of endohedral, exohedral and substitutional doped fullerene with transition metals (TM=Fe and Co atoms), which are appropriate candidates for designing magnetic devices if high spin configuration can be preserved as the ground state or if different spins can be manipulated.

We performed a comprehensive first principles study of endohedrally, exohedrally and substitutionally doped C_{60} fullerene with Fe and Co atoms and explore the structural, electronic and magnetic properties of the clusters.

In fact the Fe@C_{60} and Co@C_{60} were studied before. Tang et al. [16] studied Fe@C_{60} by BLYP [17,18] correlation-exchange function and DNP basis set. Also Salas and Valladares [19] performed density functional theory calculations on Fe@C_{60} and Co@C_{60}. However, on the one hand, in the above mentioned works the total energy inside the carbon cage is not extensively studied. On the other hand, some researchers have studied the properties of C_{59}Fe and C_{59}Co experimentally and theoretically [14,20,21]. Billas et al. [21] showed that the stable structure of Fe: C_{60} can be formed in a low pressure condensation cell through the mixing of vapor of the dopant element with vapor made of fullerenes. To the best of our knowledge, there are no comprehensive experimental

* Corresponding author.
E-mail address: m_rezaee.roknabadi@yahoo.com (M. Rezaee Rokn-Abadi).

0921-4526/$ - see front matter © 2010 Elsevier B.V. All rights reserved.
doi:10.1016/j.physb.2010.09.035

or theoretical investigations on the exohedrally doped TM: C_{60} complexes. It seems that, more studies are needed for a better understanding of the properties of TM-C_{60} systems and hence to predict their potential applications. This is the motivation for performing the calculation presented in this work.

2. Computational details

To simulate the endohedral, exohedral and substitutionally doped fullerene with the TM atom, first principles approaches using numerical atomic orbitals as basis set have been implemented. Full geometrical optimization and total energy calculations were performed with ab initio calculations based on the generalized gradient approximation (GGA) with the Perdew–Burke–Erenzerhof (PBE) functional [22] in the density functional theory and the standard norm-conserving Troullier–Martins pseudopotentials [23]. We have used the openMX code, which solves the standard Kohn–Sham equations and has been demonstrated to be very efficient for large atomic systems [24–26]. In the calculations with openMX, the same outer electrons of the TM atom were treated as valence electrons in the self-consistent field iteration. Pseudo-atomic orbitals have been constructed by using a basis set (two-s, two-p, two-d for TM and two-s and two-p for C) within 7.0 Bohr radii of the cut-off radius for confinement potential of the TM and 5.0 Bohr radii for C. The cutoffs of 150 Ry for the grid integration were utilized to represent the charge density in the real space.

To find the most stable structure of endohedral and exohedral doped fullerenes we have done single point total energy calculations. We devised five inner and outer radial paths. Each inner path starts from the cage center and extends to one of the key points on the surface of the C_{60} cage, such as atomic site (A), midpoint of the different bonds (B1, B2) and center of hexagonal and pentagonal rings (C1 and C2, respectively) as shown in Fig. 1. We refer to each path with the same designated name to the key point to which the path ends. Each external path starts from infinite toward one of the key points. For endohedral and exohedral TM-doped fullerenes, the binding energy variation is studied as a function of distance between the TM atoms and the center or the surface of the cage, respectively. The binding energy is taken as the total energy of the complexes minus the sum of the total energies of the cage and the free TM atom at infinite separation. The geometric structure of the complexes relaxed near the minimum of the binding energy by the Hellman–Feynman forces including the Pullay-like corrections. Structural optimizations were performed using the conjugate gradient algorithm until the residual forces were smaller than 0.01 eV/Å. For the heterofullerene complexes the stable geometry was obtained directly by the full geometry optimization. It was shown by previous theoretical studies [27–30] that the structure of C_{60} predicted by the DFT–GGA method is in good agreement with the experiment, hence reinforcing the reliability of the theoretical method used in the present study. Using this theoretical approach, the calculated bond lengths of C_{60} are 1.425 and 1.402 Å for single, (5–6), and double, (6–6), bonds, respectively. These are in agreement with experimental values [27,29].

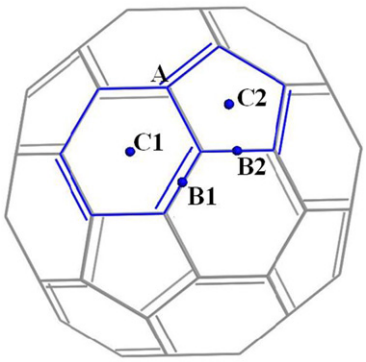

Fig. 1. Five different key points on the C_{60} surface (A, B1, B2, C1 and C2 refer to the C atom, middle of the double bond, middle of the single bond, center of the hexagon ring and center of the pentagon ring, respectively).

3. Results and discussion

3.1. Geometric structure

3.1.1. TM@C_{60} (TM=Fe, Co)

The change in the binding energy of TM atoms with respect to the internal surface of the C_{60} cage was calculated. Binding energies along all five radial paths were computed as a function of the distance from the center, and the results are shown in Fig. 2(a). As can be seen, when the Fe atoms leave the center toward the inner surface of the C_{60} cage the negative value of the binding energy increases significantly for all the examined paths A, B1, B2, C1 and C2 up to the distances of 1.15, 1.09, 1.17, 1.09 and 1.06 Å from the center, respectively. The minimum of the binding energy is related to path A (path ended to the C atom). The full geometry optimization of the Fe@C_{60} structure near the minimum of binding energy changes the distance of the Fe atom from 1.15 to 1.18 Å from the cage center with a binding energy of −1.26 eV, which indicates that the inner most stable site of the Fe atom is below the C atom of the cage.

By a similar geometric optimization process for the Co atom inside the C_{60} cage, the distance of the Co atom is obtained at 1.32 Å from the cage center along the B1 path (path ending at double bond) with the binding energy of −1.46 eV. The negative binding energy of the endohedrally doped TM atom in the C_{60} cage indicates that the complexes have thermodynamically stable structures. Also it can be seen that the binding energy of the Co atom is higher than that of the Fe atom by about 0.20 eV.

The calculated Fe–C and Co–C bond lengths are 2.32 and 2.14 Å, respectively. For both endohedrally doped TM atoms in the C_{60} cage the TM–C bond lengths are longer than the sum of TM and C atomic radii, so their interaction can be of ionic nature. C_{60} has I_h point group symmetry and all 60 atoms are equivalent. The symmetry of the TM@C_{60} (TM=Fe and Co) is C_s and C_{2v}, respectively, so their symmetry is lower than for the C_{60} case. The interaction of endohedrally doped TM atoms with the C_{60} cage changes the length of nearest single and double bonds of the C_{60} cage from 1.452 and 1.402 Å for single and double bands to 1.462 and 1.425 Å in Fe@C_{60} and 1.460 and 1.414 Å in Co@C_{60} structures.

3.1.2. TM: C_{60} (TM=Fe, Co)

The binding energy variations of the Fe atom approaching the outer surface of the cage in different paths of A–C2 are shown in Fig. 2(b). As can be seen when the Fe atom comes from infinity toward the outer surface of the C_{60} cage, the negative value of the binding energy increases for all examined paths up to the distances of 2.189, 1.96, 2.04, 2.01 and 2.09 Å from the outer surface for A, B1, B2, C1 and C2 paths, respectively. The minimum of the binding energy is related to the B1 path (path ended to the midpoint of the double bond). After full geometry optimization near the minimum of the binding energy, the distance of the Fe atom from the outer surface of the C_{60} cage is obtained as 1.92 Å with the binding energy of −1.98 eV, which indicates a most stable state of the exohedrally doped Fe atom.

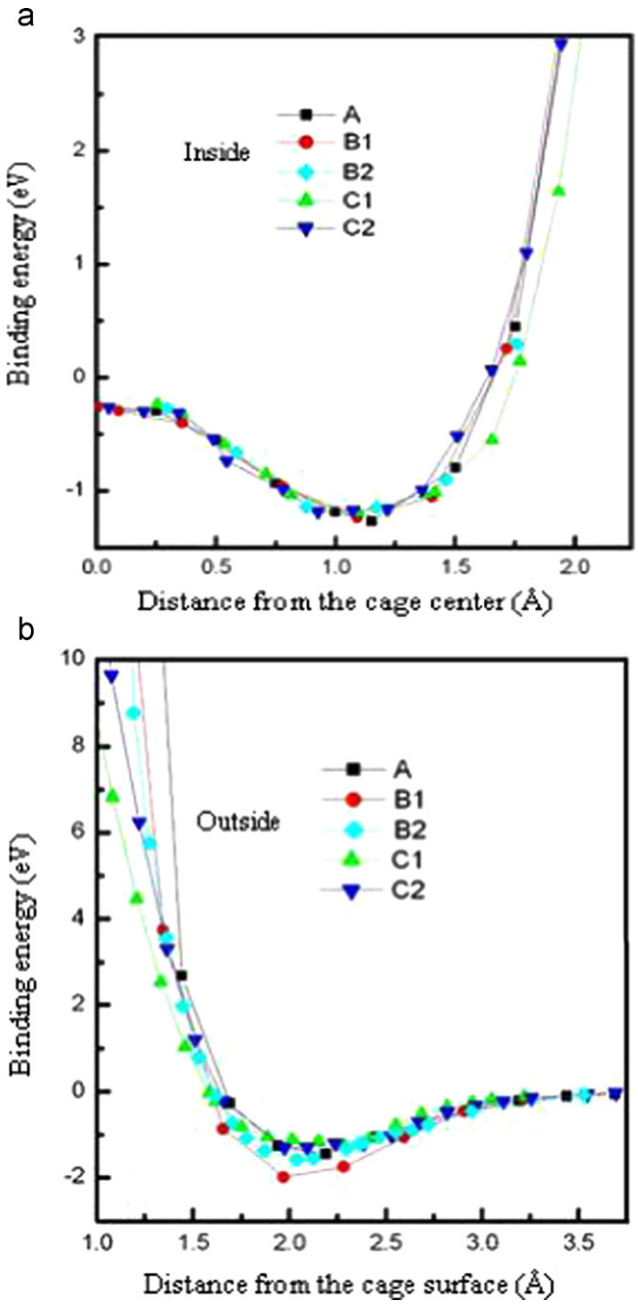

Fig. 2. The variation of the binding energy with distance of the Fe atom (a) from the cage center and (b) from the cage surface on the selected paths.

By a similar optimization process for the Co atom outside the C_{60} cage, the most stable structure is obtained when the Co atom remains at a distance of 1.84 Å from the outer surface of the cage along the B1 path with a binding energy of −2.67 eV. From the negative values of the binding energy of TM to the C_{60} fullerene it may be concluded that these complexes can be formed thermodynamically in a stable state. It is also seen that the Co atom binding energy is higher than that of the Fe atom by about 0.69 eV.

The symmetry of the TM: C_{60} (TM=Fe and Co) is C_{2v} and C_s, respectively. For both exohedrally doped TM atoms on the C_{60} cage the TM–C bond length is shorter than the sum of TM and C atomic radii, so their interaction can be of ionic and covalent natures. The lengths of the single and double bonds of the C_{60} cage near the TM atoms change from 1.452 and 1.402 to 1.462 and 1.425 Å for Fe: C_{60} and 1.504, 1.480 Å for Co: C_{60}.

3.1.3. $C_{59}TM$ (TM=Fe, Co)

The optimized geometry of $C_{59}Fe$ and $C_{59}Co$ heterofullerenes are shown in Fig. 3. When substituting one C atom with a Fe (Co) atom, the system relaxes to a less strained configuration with an energy gain of about 5.27 eV (6.1 eV). The binding energies of the relaxed structure of $C_{59}Fe$ and $C_{59}Co$ are 0.90 and 0.11 eV per atom smaller than that of C_{60}. These results indicate that the TM–C bond in $C_{59}TM$ is weaker than the C–C bond in the C_{60} structure.

The modification of the bond lengths is confined mainly to the TM–C bonds with bond lengths much greater than the corresponding C–C bond length of C_{60} as shown in Table 1. The magnitude of the deformation induced by the Fe atom is somewhat greater than that induced by the Co atom substituted on the cage surface. The reason is that the Fe atomic radius is somewhat greater than that of the Co atom [31].

3.2. Electronic and magnetic properties

Now we discuss the effect of the dopant atoms on the electronic structure of fullerene. A general feature is that all dopants introduce states in the gap between the highest occupied molecular orbital and the lowest unoccupied molecular orbital (HOMO–LUMO gap) of fullerene. First we discuss the density of states (DOS) of the most stable complexes mentioned above. In Fig. 4 we have plotted the total DOS (gray line) and the projected density of states (PDOS) on the TM-3d, 4s and 4p orbitals (solid, doted and dashed curves, respectively) for up (α) and down (β) spins. The vertical dashed line in each figure shows the HOMO (or the Fermi level, E_f) of the complex. The Gaussian broadening has been used while plotting the DOS curves and HOMO level was shifted to zero. The DOS of the C_{60} cage compared with those of the other complexes are shown in Fig. 4(a). It is found that for all complexes, additional peaks contributed by TM atomic orbitals appear in the HOMO–LUMO gap of the host cluster. From PDOS, it is clear that the mid-gap states are mainly due to the hybridization between TM-3d, 4s and 4p orbitals and the cage π orbitals. At a glance a deformation can be recognized in the DOS, including in shape and shift toward the lower energy region compared with the DOS of the C_{60} cage. This substantial shift can be explained by

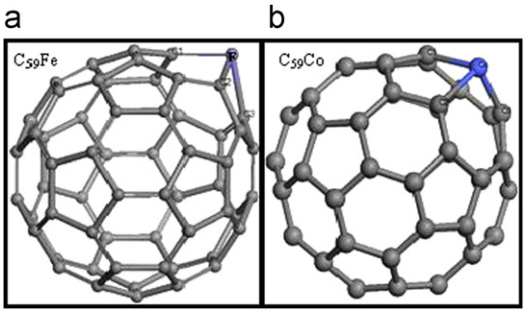

Fig. 3. The optimized geometry of (a) $C_{59}Fe$ and (b) $C_{59}Co$ heterofullerene.

Table 1
Bond lengths (Å) of $C_{59}Fe$, $C_{59}Co$ and C_{60} calculated in this work.

	$C_{59}Fe$	$C_{59}Co$
Fe–C 5–6 bonds	1.97	
Fe–C 6–6 bonds	1.84	
Co–C 5–6 bonds		1.92
Co–C 6–6 bonds		1.81
C–C 5–6 bonds	1.45–1.48	1.44–1.47
C–C 6–6 bonds	1.39–1.41	1.39–1.40

the growth of the effective Coulomb potential due to the charge transfer from the dopant atom to the cage. Furthermore, the DOS and PDOS in Fig. 4 show typical magnetic features of the considered complexes. For the Fe@C_{60} complex the HOMO level is in the α state and mainly localized on the Fe-4s orbital, while the LUMO level is in the β state and is composed of strong hybridization of Fe-3d and C-2p orbitals. According to the PDOS analysis obtained for the ground state of the exohedrally Fe-doped C_{60} complex, the α–HOMO level contains 0.44Fe-4s+0.26Fe-4p+0.3C-2p while the α-LUMO level is composed of 0.1Fe-4s+0.06Fe-3d+0.84C-2p orbitals. In the case of C_{59}Fe heterofullerene, the α- and β-HOMO, LUMO are degenerated; therefore they have the same energies. In this case the HOMO and LUMO are composed of 0.73Fe-3d+0.27C-2p and 0.33Fe-3d+0.1Fe-4p+0.57C-2p orbitals, respectively. We find that the HOMO of Co@C_{60} is in the β state and composed of 0.58Co-3d+0.42C-2p while its LUMO is in the α state and contains 0.05Co-3d+0.31Co-4s+0.1Co-4p+0.54C-2p orbitals. For the Co:C_{60} complex the β-HOMO and α-LUMO are composed of 0.47Co-3d+0.53C-2p and 0.03Co-3d+0.52Co-4s+0.26Co-4p+0.19C-2p orbitals, respectively. Also in C_{59}Co heterofullerne the α-HOMO and β-LUMO are composed of 0.21Co-3d+0.05Co-4s+0.09Co-4p+0.65C-2p and 0.24Co-3d+0.07Co-4p+0.69C-2p orbitals, respectively. The HOMO and LUMO isosurfaces of the most stable complexes considered in this work are shown in Fig. 5.

The HOMO, LUMO and HOMO–LUMO gap for all configurations are given in Table 2. The HOMO of the Fe@C_{60} is 1.65 eV higher in energy than the HOMO of C_{60}; thus the ionization is more easily realized. The LUMO of Fe@C_{60} is 0.06 eV lower in energy than the

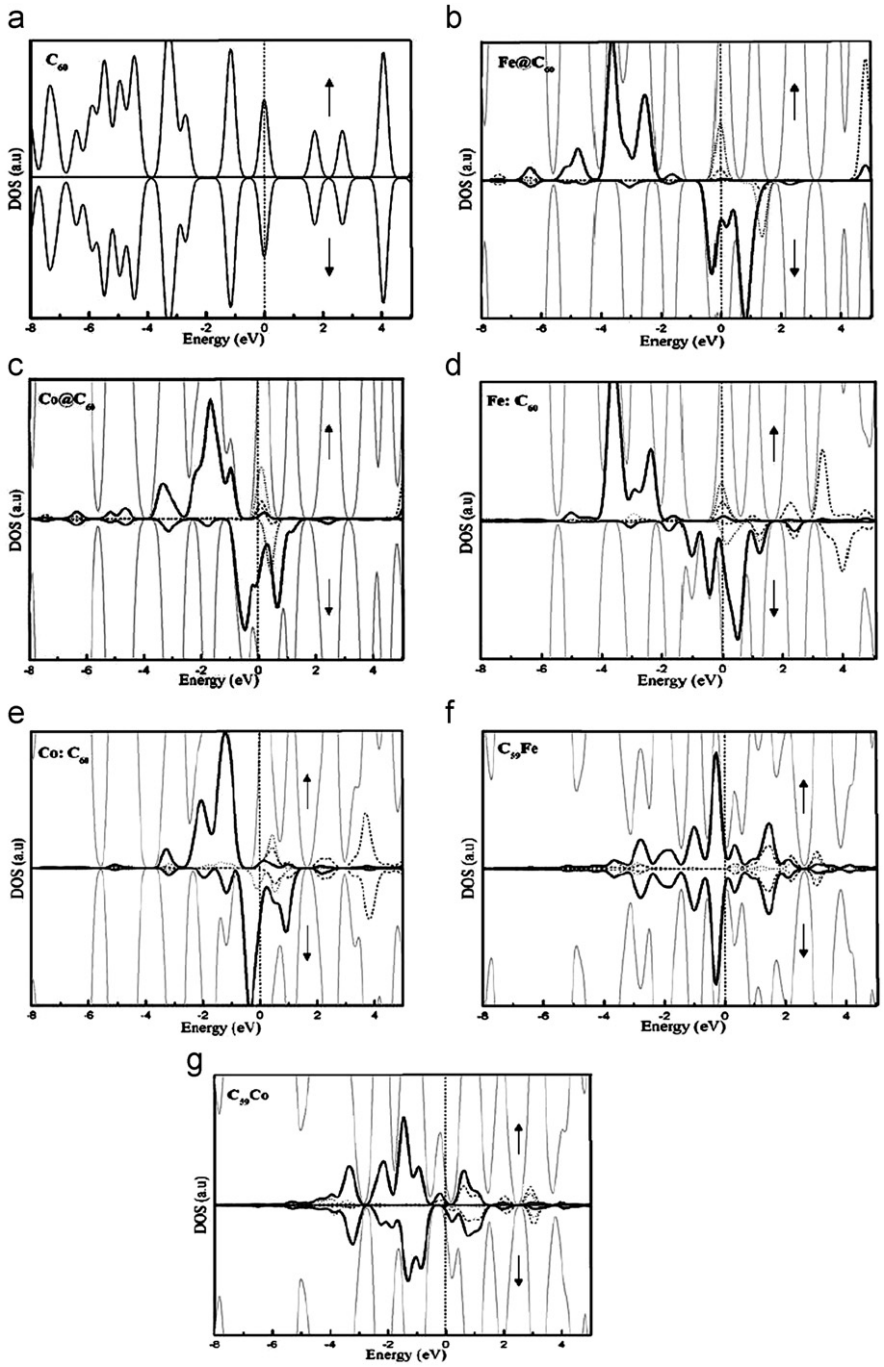

Fig. 4. The DOS of (a) C_{60}, (b) Fe@C_{60}, (c) Co@C_{60}, (d) Fe: C_{60}, (e) Co: C_{60}, (f) C_{59}Fe and (g) C_{59}Co systems.

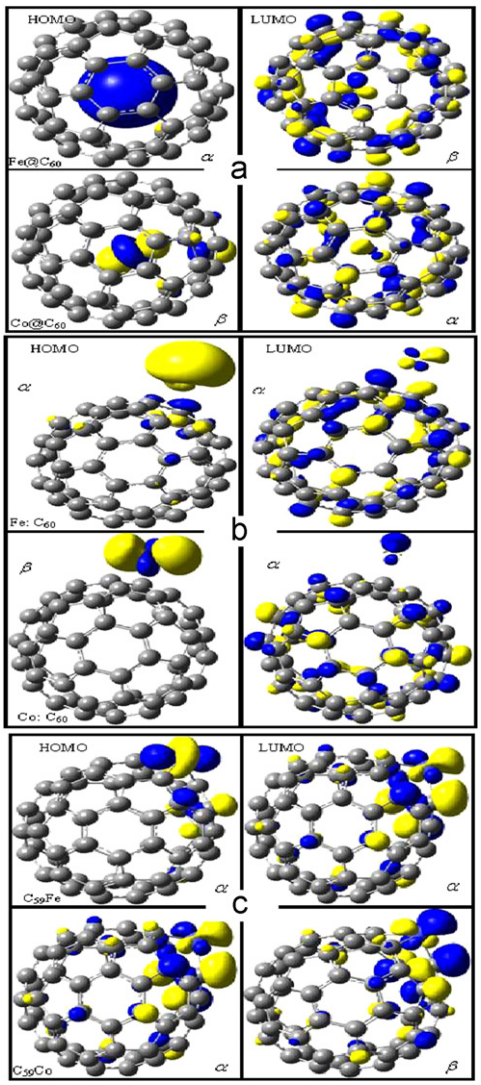

Fig. 5. The HOMO and LUMO of (a) TM@C_{60}, (b) TM: C_{60} and (c) C_{59}TM systems. The α and β exhibit the up and down spin states, respectively.

Table 2
The HOMO, LUMO and HOMO–LUMO gap of the complexes and their orbital spin states (spin up (α) and spin down (β) states).

Complexes	HOMO (eV)	LUMO (eV)	E_g
C_{60}[a]	−5.58	−3.86	1.72
Fe@C_{60}	−3.93 (α)	−3.92 (β)	0.03
Co@C_{60}	−4.07 (β)	−3.94 (α)	0.17
Fe: C_{60}	−3.98 (α)	−3.87 (α)	0.12
Co: C_{60}	−3.86 (β)	−3.65 (α)	0.21
C_{59}Fe[a]	−4.76	−4.16	0.60
C_{59}Co	−4.66 (α)	−4.24 (β)	0.42

[a] The HOMO and LUMO orbitals of the structures that degenerated by up and down spin states.

LUMO of C_{60}, so the extra electron enters the LUMO of Fe@C_{60} easily. Since the HOMO energies are recognized as an indicator of the first ionization potential (IP), the order of the first IP of the complexes is as follows: Co: C_{60} > Fe@C_{60} > Fe: C_{60} > Co@C_{60} > C_{59}Co > C_{60}. Also the LUMO energies are sometimes considered as an approximation to the electron affinities (EA). So the order of the first EA of these complexes is as follows: Co: C_{60} > C_{60} > Fe: C_{60} > Fe@C_{60} > Co@C_{60} > C_{59}Fe > C_{59}Co.

The different nature of hybridization between the TM-atomic orbitals and the C-2p orbital is well reflected in the magnitude of the local magnetic moment on the TM atom, in Table 3. We also show the total magnetic moment and the Mulliken charge population of TM valence orbitals. It can be seen that the total magnetic moments of the systems for Fe@C_{60}, Fe: C_{60} and C_{59}Fe are essentially close to the magnetic moment of the dopant atom with small magnetic moment induced on the cage in all cases. In the case of Fe@C_{60} and Fe: C_{60}, a parallel magnetic moment of $0.66\mu_B$ and an anti-parallel magnetic moment of $-0.09\mu_B$ are induced on the cage, respectively. We can see from Table 3 that the zero net spin population of Fe atom in C_{59}Fe presets the completely quenched magnetic moment of the Fe atom in C_{59}Fe heterofullerene. In the case of Co@C_{60} and Co: C_{60} anti-parallel magnetic moments of 0.61 and $0.26\mu_B$ induced on the cage decrease the total magnetic moment of the systems. In contrast, a remarkable parallel magnetic moment of $0.92\mu_B$ is induced on the C_{59}Co cage.

The key point to the magnetic moment behavior in all examined structures is the charge depletion of the TM-4s orbitals due to confinement and hybridization. As can be seen from Table 3 the enhancement of charge population in the minority TM-3d orbital that comes from 4s charge depletion determines the total magnetic moment of the systems in all cases. The TM-4s orbital charge depletions in Fe@C_{60}, Fe: C_{60} and C_{59}Fe are 52%, 65% and 62%, respectively. Also for Co@C_{60}, Co: C_{60} and C_{59}Co the 4s charge depletions are 87%, 69% and 58%, respectively. According to this charge depletion the magnetic moment of TM atom reduces in comparison with the isolated TM atom when TM interacts with the fullerene cage. However, the spin polarization enhances in the ground state of the complexes, which can be important for molecular spintronic application.

The charges on the TM atoms and their nearest neighbor C atoms are of opposite sign as shown in Fig. 6. The direction of charge transfer between the dopant atom and the carbon cage appears to be determined by their relative electronegativity. Because the C atom is more electronegative than the TM atom the electronic charge transfers from the TM to the carbon cage. Since the Fe atom transfers a part of its electron to the nearest-neighbor carbon sites, it has appreciable net positive charges of 0.410e and 0.387e in Fe@C_{60} and Fe: C_{60} complexes, respectively. In the case of C_{59}Fe heterofullerene the net charge on Fe atom is almost 0.08e.

The electronic configurations of the Fe atom in Fe@C_{60}, Fe: C_{60} and C_{59}Fe complexes are [Ar] $3d^{6.425}$ $4s^{0.968}$ $4p^{0.197}$, [Ar] $3d^{6.725}$ $4s^{0.700}$ $4p^{0.188}$ and [Ar] $3d^{6.853}$ $4s^{0.764}$ $4p^{0.304}$, respectively.

Like the Fe atom in Fe–C_{60} systems, the Co atom also transfers a part of its electron to the nearest-neighbor carbon sites; it has appreciable net positive charges of 0.367e and 0.202e in Co@C_{60} and Co: C_{60} complexes, respectively. In the C_{59}Co system the net charge on the Co atom is almost 0.09e. In the case of the Co–C_{60} systems the electronic configurations of the Co atom in Co@C_{60}, Co: C_{60} and C_{59}Co complexes are [Ar] $3d^{8.115}4s^{0.255}$ $4p^{0.263}$, [Ar] $3d^{8.017}$ $4s^{0.619}$ $4p^{0.162}$ and [Ar] $3d^{7.650}$ $4s^{0.842}$ $4p^{0.422}$, respectively.

4. Conclusion

In summary, our first principles results show that the transition metal atoms Fe and Co may form stable structures with the C_{60} fullerene. The full geometry optimization near the minimum of the binding energy curves shows that the most stable position of the Fe and Co atoms in the TM@C_{60} system is below the carbon atom and in the middle of the double bond, respectively. Also the most stable position of both Fe and Co atoms in TM: C_{60} complex is above the double bond. For all

Table 3
The magnetic properties and Mulliken population analysis of the dopant atoms.

Complex	Total magnetic moment	TM (μ_B)	4s (μ_B)	3d (μ_B)	4p (μ_B)
$Fe@C_{60}$	3.548	2.884	−0.128	2.957	0.055
Fe: C_{60}	3.376	3.469	0.466	2.953	0.050
$C_{59}Fe$	0	0	0	0	0
$Co@C_{60}$	1.004	1.623	0.013	1.589	0.021
Co: C_{60}	1.008	1.270	0.087	1.181	0.002
$C_{59}Co$	1.001	0.078	0.022	0.026	0.030

TM atom Mulliken spin population analysis

	Spin up			Spin down		
	4s	3d	4p	4s	3d	4p
Isolated Fe atom	1	5	0	1	1	0
$Fe@C_{60}$	0.420	4.691	0.126	0.548	1.734	0.071
Fe: C_{60}	0.583	4.839	0.119	0.117	1.886	0.069
$C_{59}Fe$	0.382	3.425	0.152	0.382	3.428	0.152
Isolated Co atom	1	5	0	1	2	0
$Co@C_{60}$	0.134	4.852	0.142	0.121	3.263	0.121
Co: C_{60}	0.353	4.599	0.082	0.266	3.418	0.08
$C_{59}Co$	0.432	3.838	0.226	0.41	3.812	0.196

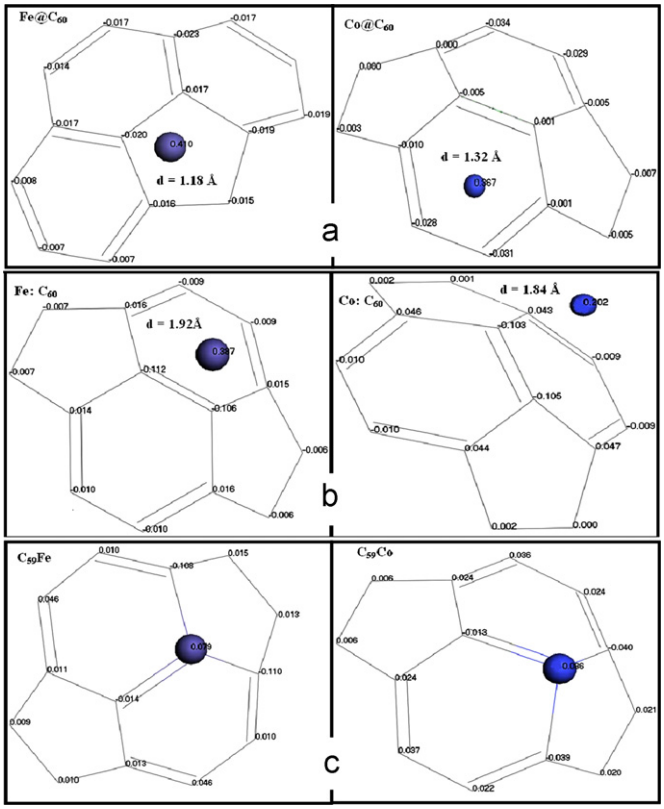

Fig. 6. Mulliken charge population analysis of the (a) $TM@C_{60}$,(b) TM: C_{60}, (c) $C_{59}TM$ systems and (d) the distance of the TM atom from the center or the surface of the endohedral or exohedral doped fullerene C_{60} cage.

examined structures, the Co atom has larger binding energy than the Fe atom. For all complexes, additional peaks contributed by TM-3d, 4s and 4p states appear in the HOMO–LUMO gap of the host cluster. The mid-gap states are mainly due to the hybridization between TM-3d, 4s and 4p orbitals and the cage π orbitals. Due to the charge depletion of TM-4s orbital to TM-3d and 4p orbitals, the magnetic moment of TM atom reduces by interacting with the fullerene cage. Because the C atom is more electronegative than the TM atom overall charge transfer occurs from TM atoms to the carbon cage.

References

[1] H.W. Kroto, J.R. Heath, S.C.Ó. Brien, R.F. Curl, R.E. Smalley, Nature 318 (1985) 162.
[2] P.W. Fowler, D.E. Manolopoulos, in: An Atlas of Fullerenes, Oxford University Press, Oxford, 1995.
[3] A. Gromov, N. Krawez, A. Lassesson, D.I. Ostrovskii, E.E.B. Campbell, Currr. Appl. Phys. 2 (2002) 51.
[4] C. Knapp, N. Weiden, K. Käss, K.-P. Dinse, B. Pietzak, M. Waiblinger, A. Weidinger, Mol. Phys. 95 (1998) 999.
[5] C. Knapp, K.-P. Dinse, B. Pietzak, M. Waiblinger, A. Weidinger, Chem. Phys. Lett. 272 (1997) 433.
[6] T.A. Murphy, T. Pawlik, A. Weidinger, M. Höhne, R. Alcala, J.–M. Spaeth, Chem. Phys. Lett. 77 (1996) 1075.
[7] K. Winkler, A.B. Dias, A.L. Balch, Chem. Mater. 12 (2000) 1386.
[8] X.Y. Ren, Z.Y. Liu, T.Q. Zhu, X.H. Wen, X.H. Guo, J. Mol. Struct.: Theochem. 664 (2003) 247.
[9] A.F. Hebard, M.J. Rosseinsky, R.C. Haddon, D.W. Murphy, S.H. Glarm, T.T.M. Palstra, A.P. Ramirez, A.R. Kortan, Nature 350 (1991) 600.
[10] J. Lu, Y. Zhou, Y. Luo, Y. Huang, X. Zhang, X. Zhao, Mol. Phys. 99 (2001) 1203.
[11] A.H.H. Chang, W.C. Ermler, R.M. Pitzer, J. Chem. Phys. 94 (1991) 5004.
[12] K.E. Laasonen, W. Andreoni, M. Parrinello, Science 258 (1992) 1916.
[13] V.N. Ivanova, J. Struct. Chem. 41 (2000) 135.
[14] W. Branz, I.M.L. Billas, N. Malinowski, F. Tast, M. Heinebrodt, T.P. Martin, J. Chem. Phys. 109 (1998) 3425.
[15] J. Lu, R.F. Sabirianov, W.N. Mei, Y. Gao, C.–G. Duan, X. zeng, J. Phys. Chem. B 110 (2006) 23637.
[16] C.–M. Tang, K.–M. Deng, J.–L. Yang, X. Wang, Chin. J. Chem. 24 (2006) 1133.
[17] A.D. Becke, Phys. Rev. A 38 (1998) 3098.
[18] C. Lee, W. Yang, R. Parr, Phys. Rev. B 37 (1998) 785.
[19] R.E.E. Salas, A.A. Valladares, J. Mol. Struct.: Theochem. 869 (2008) 1.
[20] C.G. Ding, J.L. Yang, X.Y. Cui, J. Chem. Phys. 111 (1999) 8481.
[21] I.M.L. Billas, W. Branz, N. Malinowski, F. Tast, M. Heinebrodt, T.P. Martin, C. Massobrio, M. Boero, M. Parrinello, Nanostruct. Mater. 12 (1999) 1071.
[22] J.P. Perdew, K. Burke, M. Ernzerhof, Phys. Rev. Lett. 77 (1996) 3865.
[23] N. Troullier, J.L. Martins, Phys. Rev. B 43 (1991) 1993.
[24] T. Ozaki, Phys. Rev. B 67 (2003) 155108.
[25] T. Ozaki, H. Kino, Phys. Rev. B 69 (2004) 195113.
[26] T. Ozaki, H. Kino, Phys. Rev. B 72 (2005) 045121.
[27] O.V. Pupysheva, A.A. Farajian, B.I. Yakobson, Nano Lett. 8 (2008) 3.
[28] K. Hedberg, L. Hedberg, D.S. Bethune, C.A. Brown, H.C. Dron, R.D. Johnson, M. Devries, Science 254 (1991) 410.
[29] A.V. Nikolaev, T.J.S. Dennis, K. Prassides, A.K. Soper, Chem. Phys. Lett. 223 (1994) 143.
[30] S.M. Lee, R.J. Nicholls, D. Nguyen-Manh, D.G. Pettifor, G.A.D. Briggs, S. Lazar, D.A. Pankhurst, D.J.H. Cockayne, Chem. Phys. Lett. 404 (2005) 206.
[31] J.A. Dean, in: Lange's Handbook of Chemistry, McGraw-Hill, New York, 1999; G.J. Marshall, Mater. Sci. Forum. 19 (1996) 217.